An integrated approach to monitor the calibration stability of operational dual-polarization radars

ARTICLE · FEBRUARY 2016

DOI: 10.5194/amt-2016-36

5 AUTHORS, INCLUDING:

Renzo Bechini

Regional Environmental Protection Agency…

53 PUBLICATIONS **166** CITATIONS

SEE PROFILE

Cremonini Roberto

Regional Environmental Protection Agency…

74 PUBLICATIONS **170** CITATIONS

SEE PROFILE

Claudio Cassardo

Università degli Studi di Torino

114 PUBLICATIONS **405** CITATIONS

SEE PROFILE

Atmos. Meas. Tech. Discuss., doi:10.5194/amt-2016-36, 2016
Manuscript under review for journal Atmos. Meas. Tech.
Published: 15 February 2016

Atmospheric Measurement Techniques Discussions

An integrated approach to monitor the calibration stability of operational dual-polarization radars

Mattia Vaccarono[1], Renzo Bechini[1,2], Venkatachalam Chandrasekar[1], Roberto Cremonini[2], and Claudio Cassardo[3]

[1]Colorado State University, Fort Collins, Colorado
[2]Arpa Piemonte, via Pio VII 9, Torino, Italy
[3]Università degli Studi di Torino, via Pietro Giuria 1, Torino, Italy

Correspondence to: Mattia Vaccarono (mvaccar[at]engr.colostate.edu)

Abstract. The stability of the weather radar calibration is a mandatory aspect for quantitative applications, such as rainfall estimation, short-term weather prediction and initialization of numerical atmospheric and hydrological models. Over the years, calibration monitoring techniques based on external sources have been developed, specifically the calibration using the Sun, and the calibration based on ground clutter returns. In this paper, these two techniques are integrated and complemented with a self-consistency procedure and an intercalibration technique. The aim of the integrated approach is to implement a robust method for online monitoring, able to detect significant changes in the radar calibration. The physical consistency of polarimetric radar observables is exploited using the self-consistency approach, based on the expected correspondence between the dual-polarization power and phase measurements in rain. This technique allows to provide a reference absolute value for the radar calibration, from which eventual deviations may be detected using the other procedures. In particular, the ground clutter calibration is implemented on both polarization channels (horizontal and vertical) and for each radar scan, allowing to monitor the polarimetric variables and promptly recognize hardware failures. The Sun calibration allows to monitor the calibration and sensitivity of the radar receiver, in addition to the antenna pointing accuracy. It is also applied using observations collected during the standard operational scans, but requires longer integration times (several days) in order to accumulate a sufficient amount of data. Finally, an intercalibration technique is developed and performed to compare co-located measurements collected in rain by two radars on overlapping regions. The integrated approach is performed on the C-band weather radar network in northwestern Italy, during July - October 2014. The set of methods considered is shown to provide a robust online tool to monitor the stability of the radar calibration. The attainable accuracy for the calibration of the radar reflectivity is about 1dB, which is considered adequate for most quantitative applications.

Keywords. weather radar, data quality, calibration stability, polarimetry, self-consistency

1 Introduction

Weather radar data are used for precipitation monitoring but also for quantitative applications, such as rainfall estimation, short-term weather prediction and initialization of numerical atmospheric and hydrological models. Therefore, the data quality

Atmos. Meas. Tech. Discuss., doi:10.5194/amt-2016-36, 2016
Manuscript under review for journal Atmos. Meas. Tech.
Published: 15 February 2016

Atmospheric Measurement Techniques Discussions

of radars must be ensured and continuously monitored. Specifically, the stability of the radar calibration is a mandatory aspect for performing reliable rainfall measurements. Over the years, many calibration techniques based on external sources have been developed, e.g. calibration with the Sun, and based on fixed and well-known targets, e.g. calibration with ground clutter echoes. The calibration using the solar interferencens has been first proposed by Whiton et al. (1976) and then it has been applied on operational radars for the monitoring of the radar receiver chain and antenna pointing (Holleman and Beekhuis (2004), Holleman et al. (2010), Gabella et al. (2014) and Altube et al. (2015)). The ground clutter calibration allows to monitor automatically the stability of the radar calibration, specifically the transmitting and receiving chain of both polarization channels, through statistical analysis of the echo power return from fixed targets (Silberstein et al. (2008) and Wolff et al. (2015)).

For a radar network, the stability of the radar calibration can also be monitored considering the joint observations in rain medium collected by two or more radars. This intercalibration ensures the consistency and stability of the precipitation measurements comparing the radar reflectivity values of two or more radars in the same area. The areas are computed from the intersection of the radar beams with a theoretical model. An operational intercalibration of the two C-band radars managed by Arpa Piemonte is performed on a daily basis, when enough meteorological echoes are available in the overlapping region, by comparing the volume scan intersecting bins. This check provides a useful way to detect eventual drift of one's radar calibration.

In addition, a self-consitency procedure can be performed to evalute the absolute radar calibration in case of heavy rain. Gorgucci et al. (1992) and Scarchilli et al. (1996) proposed and developed a procedure based on the radar reflectivity at horizontal polarization (Z_H), differential reflectivity (Z_{dr}) and specific differential phase shift (K_{dp}), known as self-consistency since these three radar observables lie in a limited three-dimensional space for rain medium.

In this paper we propose an integrated approach to monitor the calibration stability of operational radars based on the above mentioned calibration techniques. The paper is organized as follows. Section 2 describes the radars and the data on which the proposed approach for the online calibration monitoring is performed. Section 3 reviews the self-consistency procedure for the radar absolute calibration and the calibration monitoring techniques, namely intercalibration, ground clutter calibration and Sun calibration. The results of each calibration technique are discussed in Sect. 4. In Sect. 5, the integrated approach to monitor the calibration stability of operational radars is discussed and the conclusions are drawn.

2 Data

The calibration monitoring of the Arpa Piemonte C-band weather radars is evaluated for the period between 28 July 2014 and 13 October 2014 on the operational volume scans. The absolute calibration of the radars is checked using the self-consistency procedure during the first and last day of the study period, which have been chosen with proper meteorological conditions. During the whole period, the radar calibration is monitored using the ground clutter calibration, the Sun calibration and the intercalibration procedures.

Atmos. Meas. Tech. Discuss., doi:10.5194/amt-2016-36, 2016
Manuscript under review for journal Atmos. Meas. Tech.
Published: 15 February 2016

Atmospheric Measurement Techniques Discussions

2.1 Arpa Piemonte C-band weather radars

The continuous surveillance of the territory in the north-western region of Italy is operated by the Regional Agency for environmental protection (Arpa) Piemonte, which manages two C-band weather radars and a mobile X-band radar for research purposes. The two C-band radars are located at Bric della Croce hill near Turin and at Monte Settepani mountain near Savona in Liguria region (Table 1 and Fig. 1) Bric della Croce radar is located on the hills near Turin, at 736 meters above sea level. It is placed on the top of a 33 meters height tower and covers the Piemonte region. The East side of the radar domain does not present obstacles that may block the radar beam, while, in the Western side of the radar domain, the visibility is limited by the Alps and, in the Southern side, by the Apennines. The radar of Bric della Croce performs a volume scans every 5 minutes. However, due to different filter settings on the scans starting at minute 0 and 5, for the purpose of this study only the scan starting at minute 0 is considered. The scan is composed of 11 elevations between -0.1 and 28.5 degrees. The volume scan is polarimetric and the observed parameters are: radar reflectivity Z_H, differential reflectivity Z_{dr}, correlation coefficient ρ_{hv}, differential phase shift Φ_{dp}, and the Doppler velocity V. Each measure is the result of the integration of about 50 pulses. The range of the volume scan is 170km and the range resolution is 340m. The angular resolution is 1 degree. The pulse time width is 0.5μs (short pulse). Bric della Croce radar operates in dual-PRF mode to mitigate the radar dilemma, with frequencies 882 and 588 Hz.

The second C-band weather radar is located on the top of Monte Settepani mountain at 1386m asl, in the Ligurian Apennines. This radar is managed by Arpa Piemonte in collaboration with the Ligurian Region. This strategic position allows to monitor the precipitations coming from the Mediterranean sea, which may cause severe hydrological effects. Furthermore, Monte Settepani radar has an excellent visibility in the North and East sectors, corresponding to the Po valley and the mountain areas of Piemonte. Monte Settepani radar performs a volume scans every 10 minutes. The volume scan is polarimetric and the acquired parameters are the same as for the Bric della Croce radar. The volumetric scan is composed by seven elevations between -0.3 and 14.9°. The range is 136km and the range resolution is 375m, using short pulses of 0.5μs and PRF of 1,090Hz.

The specific differential phase shift K_{dp} is operationally calculated for both systems using the Wang and Chandrasekar (2009) algorithm. After K_{dp} estimation, a hydrometeor classification is performed on the dual polarization observations (Bechini and Chandrasekar, 2015). The output of the classification is used to select the data for the different calibration procedures. In order to account for the effects of attenuation and differential attenuation, the rain profiling algorithm based on (Testud et al., 2000) is applied to correct the horizontal reflectivity for path attenuation, while differential attenuation is linearly estimated from the horizontal attenuation (Bringi et al., 1990).

Table 2 reports the relevant characteristics of the systems.

3 Integrated approach for radar online calibration

The calibration techniques are often investigated separately and the task of each technique is the monitoring of a section of the radar system. The Sun calibration performs the monitoring of the radar receiving chain and the antenna pointing, using the Sun as natural radio source. The ground clutter calibration is able to monitor the calibration stability of the radar transmitting

Atmos. Meas. Tech. Discuss., doi:10.5194/amt-2016-36, 2016
Manuscript under review for journal Atmos. Meas. Tech.
Published: 15 February 2016

Atmospheric Measurement Techniques Discussions

together with the receiving chain. Nevertheless, in case of loss of calibration in the radar transmitting chain, the ground clutter calibration is not able to detect whether the loss of calibration affects the transmitting or receiving chain. Combining and comparing the Sun calibration together with the ground clutter calibration, it is possible to retrieve additional information about the eventual calibration change.

Moreover, to monitor the calibration stability of operational radars during precipitation, the intercalibration may be performed when a radar network is available. The intercalibration procedure allows to compare the reflectivity measurements acquired by two radars over the same area.

The intercalibration, the Sun and ground clutter calibration, however, only allow to monitor the eventual deviation of the radar calibration from a given reference value. Hence, it is required to verify the absolute calibration of the radar by the self-consistency procedure. The integrated approach involves the following procedures:

- self-consistency, performed during selected heavy rainfall events;
- intercalibration, performed whenever precipitation is detected on overlapping area;
- ground clutter calibration, performed daily;
- Sun calibration, performed every five days, on the previous five days.

3.1 Self-consistency

The polarimetric radar measurements of rainfall are in self-consistency (Scarchilli et al., 1996), since Z_H, Z_{dr} and K_{dp} lie in a limited three-dimensional space for rain medium. Among the triplet of measurements Z_H, Z_{dr} and K_{dp}, the self-consistency technique allows to obtain estimates of one of the parameters based on the other two. Dual polarization estimate of rainfall can be done by two methods: one based on the reflectivity measurement at horizontal polarization and on the differential reflectivity, and one based on the specific differential propagation phase measurement. This latter estimator is assumed to be unbiased, since it is based on phase measurements, so it is immune to calibration issues (Gorgucci et al., 1992).

The distribution of drop sizes (DSD) and shapes are fundamental for deriving physically based rain rate algorithms. The raindrop size distribution describes the probability density (distribution function) of raindrops. A gamma distribution model (or a similar model such as log-normal distribution) can adequately describe many of the natural variations in the shape of raindrop size distributions (Ulbrich, 1983). For polarimetric radars, the three radar measurements Z, Z_{dr} and K_{dp} can be used in various combinations to estimate rain rate. These estimators are based on the Beard-Chuang equilibrium shape model (Beard and Chuang, 1987), which describes the oblate shape of the rain drops. The two radar rainfall algorithm used in this study are namely $R_{dr}(Z, Z_{dr})$ and $R_{dp}(K_{dp}, Z_{dr})$.

A robust rain rate estimator can be constructed using z_{dr} ($z_{dr} = 10^{0.1 Z_{dr}}$) of the form,

$$R_{dr} = c_1 Z_h^{a_1} 10^{0.1 b_1 Z_{dr}} \quad (1)$$

where Z_h is in units of $mm^6 m^{-3}$ and Z_{dr} is in dB (Gorgucci et al., 1992). Coefficients a_1, b_1 and c_1 at C-band (5.45GHz) are 0.91, -2.09 and 5.8×10^{-3}, respectively (Bringi and Chandrasekar, 2001).

Atmos. Meas. Tech. Discuss., doi:10.5194/amt-2016-36, 2016
Manuscript under review for journal Atmos. Meas. Tech.
Published: 15 February 2016

Atmospheric Measurement Techniques Discussions

Using the specific differential propagation phase and since K_{dp} is inversely proportional to wavelength in Rayleigh limit, a general $R(K_{dp})$ estimator can be written using a frequency-scaling argument in the form (Bringi and Chandrasekar, 2001):

$$R_{dp} = 129 \left(\frac{K_{dp}}{f} \right)^{b_2} \tag{2}$$

where the unit of R_{dp} is $mm\ h^{-1}$, K_{dp} is in $degkm^{-1}$ and f is in GHz. At 5 GHz frequency it reduces to

$$R_{dp} = 32.8(K_{dp})^{0.85} \tag{3}$$

According to Gorgucci et al. (1992), the absolute calibration bias can be computed as a function of the slope of the scatterplot between R_{dp} and R_{dr}. Let θ the angle of the position vector formed by the coordinates of R_{dp} and R_{dr}. It follows that $tan(\theta)$ can be estimated as the slope of a linear model applied on the rain rate pairs. The system gain bias can be expressed in dB scale as:

$$B(dB) = -\frac{10}{a_1} Log(tan(\theta)) \tag{4}$$

where $10Log(tan(\theta))$ is the slope of the linear regression computed in dB scale.

3.2 Intercalibration

The intercalibration ensures the consistency and stability of the precipitation measurements comparing the radar reflectivity values of two or more radars operating in the same frequency band, over the same area and time. The areas are computed from the intersection of the radar beams with a theoretical model. The operational intercalibration of the two C-band radars is performed when sufficient meteorological echoes are available in the overlapping area. This procedure is able to detect eventual calibration drift. In order to compare measurements from different radars, the different viewing geometry should be carefully considered. The overlapping volumes are evaluated theoretically for each elevation of both considered radars. Ideally, the pair of radar cells ($\sim 1^\circ \times 0.3$km) should have similar size in order to obtain consistent results from the intercalibration. However, to increase the number of radar cells on which the intercalibration can be performed, tolerances on the altitude of the main beam center and on the distance from the radars are applied. The height from the ground (or sea level) of the radar beam is computed by:

$$h_{_{beam}} = \sqrt{s_r^2 + (h_0 + R_E)^2 + 2 s_r (h_0 + R_E) sin\theta} - R_E \tag{5}$$

where s_r is the slant range (i.e., the range along the beam), h_0 the radar height above the sea level and R_E the effective Earth radius. Considering the 3dB beam width of Bric della Croce and Monte Settepani antennas and the distance between the two radars, an example of vertical section of the two radar beam is displayed in Fig. 2a. The displayed elevations are 1.2° (Bric della Croce) and 0.7° (Monte Settepani) and the direction is SSE for Bric della Croce and NNW for Monte Settepani.
The vertical tolerance is set to 100m above and below the intersection of the two main beam axes. To select radar cells with similar volume, a threshold is imposed on the difference of the distances between the selected cell and the two radars.

Atmos. Meas. Tech. Discuss., doi:10.5194/amt-2016-36, 2016
Manuscript under review for journal Atmos. Meas. Tech.
Published: 15 February 2016

Atmospheric Measurement Techniques Discussions

When projected on the ground, this value must not exceed 40km. For each pair of elevations in the scan strategy of the two radars, intersecting bins in the overlapping area are computed. The beam height is calculated on a spatial grid in geographical coordinates and the cells where the difference between the beam heights is below the tolerance are selected. The position of the detected cells is then converted from geographical coordinates to bin-azimuth coordinates of each radar.

The Bric della Croce radar is located at 736m above sea level near Turin, while the Monte Settepani radar at 1386m in the Ligurian Apennines. One of the most suitable pair of elevation scans is represented in Fig. 2b, where the beam height of Bric della Croce scan at 1.2° and Monte Settepani scan at 0.7° is shown. Due to the different radar altitudes, the second elevation scan of Monte Settepani is combined with the third elevation scan of Bric della Croce radar and the altitude of the main beam center axis is about 2,500m. The overlapping volume that satisfies the vertical tolerance is displayed in blue and it is located approximately above the Cuneo plain and Asti hills. Considering all elevation pairs, the total number of intersections that satisfy the imposed geometrical conditions is about 10^5.

The intercalibration procedure then requires a statical Look-Up Table (LUT) to store the polar coordinates of the intersecting bins. For these selected bins, the corresponding radar observations are extracted from the polar volumes. In addition to the reflectivity, the correlation coefficient ρ_{hv} is also considered in the analysis to select only rain measurements. Finally, to avoid considering observations in regions where the radar beam is blocked by the orography, a Digital Elevation Model (DEM) is adopted to simulate the radar visibility along the radials.

3.3 Ground clutter calibration

The aim of the ground clutter calibration is to extract information about the radar system calibration from well-know targets. The ground clutter calibration uses a large set of echoes from ground clutter at low elevation scans to provide a stable reference Empirical Cumulative Distribution Function (ECDF) of clutter reflectivity. The statistical approach is needed since clutter echoes may vary over time. e.g. due to wind, vegetation changes or snow coverage. The ground clutter calibration allows to monitor the stability over time of the radar calibration considering the value where the ECDF reaches the 95^{th} percentile (Silberstein et al., 2008). In this paper, this techniques has been applied to both polarization channels of polarimetric weather radars.

The key points of the ground clutter calibration have been stated by Silberstein et al. (2008) and the success of the procedure depends on:

- the ground returns stability,
- the stability of elevation angle at which the clutter echoes are measured,
- the rainfall rate; the precipitation echoes must not dominate the clutter echoes.

When these conditions are met, surface clutter echoes can be used in the ground clutter calibration because of their limited variability over time. Different samples have different ECDF but the values at which the ECDF reaches 0.95 should not change over time for a given radar system (Silberstein et al., 2008).

Atmos. Meas. Tech. Discuss., doi:10.5194/amt-2016-36, 2016
Manuscript under review for journal Atmos. Meas. Tech.
Published: 15 February 2016

Atmospheric Measurement Techniques Discussions

The method of the ground clutter calibration is based on a clutter mask, that is used to select clutter echoes that appear very frequently in the radar images. This is intended to minimize the possible contamination by meteorological echoes (Silberstein et al. (2008) and Wolff et al. (2015)). The radar volume scans without meteorological echoes are processed on a daily basis to calculate a map of the average clutter reflectivity and a map of the frequency of occurrence of the clutter echoes. In order to avoid sudden clutter modifications, both maps are averaged with the corresponding maps from the previous days. The clutter masks are generated for each elevation of the volume scan and for each operational radar.

The clutter masks of Bric della Croce radar, at the lowest elevation, are shown in figures 3a and 3b. Most of the clutter echoes have a mean frequency above 95% (Fig. 3b), meaning that there were no significant changes in their spatial distribution. The Alps are the most important source of clutter, whose reflectivity may exceed 65dBZ in some areas (Fig. 3a). The mean value and the frequency of clutter echoes for Monte Settepani radar are shown in figures 3c and3d.

3.4 Sun calibration

The calibration of radar systems using the Sun as radio source was first proposed by Whiton et al. (1976) and developed in several works by Tapping (2001a), Holleman and Beekhuis (2004), Holleman et al. (2010), Gabella et al. (2014) and Altube et al. (2015). The Sun is used for monitoring the receiver calibration, alignment of the radar antenna and checking the antenna gain (Rinehart, 2004). According to Holleman et al. (2010), the antenna elevation and effective receiver system gain could be determined within 0.2° and 1.3dB, respectively. The peculiarities of the Sun as natural microwave source are:

- 0.54° apparent angular diameter
- differential reflectivity about 0dB, because the radiation is not polarized
- in radar polar plot (azimuth-range), the solar interference appears as an uniform signal along one or more radials

The Sun calibration is performed on reflectivity and differential reflectivity data. The method proposed by Holleman et al. (2010) does not require to stop the operational radar scans (i.e. the Sun tracking task requires to stop the normal radar operations) because it seeks the solar rays intercepted during the operational scanning. The Sun position is computed theoretically at the radar location and then it is converted in azimuth and range bins. The automated routine scans the rays in the region (defined by an azimuthal tolerance) where the Sun should be seen by the radar. If the fraction of valid bins inside the detected ray is higher than typically 0.9 and the standard deviation of the computed power is less than 1dB, the ray is flagged as solar ray (Holleman and Beekhuis, 2004).

The Sun elevation is corrected for the atmospheric refraction (Holleman et al., 2010). The calculated correction is maximum at zero elevation, but never exceeds 0.5°. The solar flux is continuously monitored at S-band by the Dominion Radio Astrophysical Observatory (DRAO) in Canada. The current solar flux is obtained from the ftp server of DRAO observatory: ftp://ftp.geolab.nrcan.gc.ca/data/solar_flux/daily_flux_values/fluxtable.txt. The solar flux is given in solar flux units: $1sfu = 10^{-22} W\, m^{-2}\, Hz^{-1}$. The S-band solar flux measurements can be applied to other frequencies with an accuracy of

Atmos. Meas. Tech. Discuss., doi:10.5194/amt-2016-36, 2016
Manuscript under review for journal Atmos. Meas. Tech.
Published: 15 February 2016

Atmospheric Measurement Techniques Discussions

roughly 1dB. The reference solar flux is converted at the radar band (C-band) by Eq. (6), (Tapping, 2001b).

$$F_C = 0.71 \times (F_S - 64) + 126 \ \ (sfu) \tag{6}$$

The estimated solar power P_{Sun} received by the radar is given by:

$$P_{Sun} = \frac{1}{2} 10^{-13} \Delta f \, A \, F_C \ \ (W) \tag{7}$$

where Δf is the bandwidth of the radar receiver in MHz and A is the effective area of the antenna in m^2. The factor $1/2$ takes into account the unpolarized nature of the Sun, while the radar separately receives the horizontal and vertical polarized components of the incoming radiation. The estimated received solar power is compared with the solar power measured by the radar. The solar power is computed by the radar equation from the radar reflectivity measured at a given range:

$$P\,(dBm) = Z\,(dBZ) - 20Log(R) - 2a\,R - C \tag{8}$$

where *R* is the range (km), *C* the radar constant (dB) and *a* the one-way gaseous attenuation in dB. The received solar power has to be corrected for the gaseous attenuation between the radar antenna and the top of the atmosphere (TOA), for the imperfect overlap with the antenna sensitivity pattern and for the averaging of the received power while the antenna is rotating (Holleman and Beekhuis, 2004). The solar power received by the radar can be fit to a theoretical model, in which the received power is represented by a Gaussian function. The model proposed by Holleman et al. (2010) and discussed by Altube et al. (2014, 2015) is given by:

$$P_{det} = A_{gas} A_{avg} P_{TOA} e^{-4ln(2)\left[\frac{(az-az_{bias})^2}{\Delta_r^2} + \frac{(el-el_{bias})^2}{\Delta_r^2}\right]} \tag{9}$$

where the solar power received by the radar P_{det} and the power at the top of the atmosphere P_{TOA} are in mW, A_{avg} dimensionless and $A_{gas} = 10^{(a/10)}$. The three model parameters are the power at the top of the atmosphere as seen by the radar P_{TOA}, the azimuthal bias az_{bias} and the elevation bias el_{bias}. The biases represent the antenna pointing deviation and they are computed from the difference $\Delta azimuth = az_{radar} - az_{Sun}$ and $\Delta elevation = el_{radar} - el_{Sun}$. The difference between the radar and Sun elevations is corrected by:

$$\Delta azimuth = (el_{radar} - el_{Sun}) \times cos(el_{radar}) \tag{10}$$

where $cos(el_{radar})$ projects the incline plane on the horizontal plane. Operatively, the fit is computed by the Nonlinear Least Square method, whose outputs are the fit parameters, their uncertainties and the fit residual standard error.

4 Results

The stability of the radar calibration is evaluated for the period between 28 July 2014 and 13 October 2014. The self-consistency technique is adopted to ensure the absolute calibration of the radars at the beginning and at the end of the study period. During the analyzed period, when the precipitation data are not suitable to perform the self-consistency, the clutter and Sun calibration allow to monitor the stability of the calibration.

Atmos. Meas. Tech. Discuss., doi:10.5194/amt-2016-36, 2016
Manuscript under review for journal Atmos. Meas. Tech.
Published: 15 February 2016

Atmospheric Measurement Techniques Discussions

4.1 Radar absolute calibration with self-consistency

The application of the self-consistency technique requires that Z_{dr} is properly calibrated (Gorgucci et al., 2001). In order to verify the calibration of Z_{dr} we considered all measurements collected matching the following criteria:

- observations in liquid phase, as inferred from the application of the hydrometeor classification
- $\rho_{hv} > 0.99$
- horizontal reflectivity between 10 and 20dBZ

Using the above mentioned criteria results in selecting echoes from drizzle composed by nearly spherical droplets and expected differential reflectivity close to 0dB or slightly positive. The histograms in Fig. 4 and Fig. 5 show a roughly symmetric distribution with the most populated class being the one comprised between 0 and 0.2dB for both systems. Therefore, Z_{dr} is considered to be properly calibrated and the self-consistency technique may be performed. Data are collected in rain and filtered according to the Z_{dr} (>0dB) and ρ_{hv} (>0.98) values to select proper meteorological echoes. The simple scheme adopted for the correction of differential attenuation (Sect. 2.1) may not be adequate when observations are affected by strong attenuation. For this reason, the data are removed from the analysis where $Z_{dr} < 0dB$, since negative value of differential reflectivity are unphysical in rain media. The co-polar correlation coefficient ρ_{hv} is in general $\gtrsim 0.98$ for raindrops and $\lesssim 0.7$ for clutter echoes. Considering a conservative estimation of the co-polar correlation coefficient in rain, data with $\rho_{hv} < 0.9$ are removed from the dataset. The rain rates described previously (Eq. (1) and (3)) are computed on the 10 minute scans at 0.5° for Bric della Croce and 0.7° for Monte Settepani for the whole day. The rain rate estimation based on Z_H and Z_{dr} is compared to the K_{dp}-based rain rate, which is considered unbiased. The results are presented as density scatter plot of the rain rates in logaritmic scale, with the colors displaying the density of data. A linear fit with 1:1 slope is computed to estimate the intercept value, which is then converted to the system bias using Eq. (4). Since K_{dp} in light rain is noisy, inclusion of these data may affect the regression results. The standard deviation of estimated K_{dp} in drizzle ($\sigma_{drizzle}(K_{dp})$), where K_{dp} is expected to be nearly $0 deg km^{-1}$, is assumed as the noise level. For both systems we found $\sigma_{drizzle}(K_{dp}) \simeq 0.4 deg km^{-1}$. From Eq. (3), the corresponding rain rate value is:

$$R_{min} = 32.8(\sigma_{drizzle}(K_{dp}))^{0.85} \simeq 14\ mm\,hr^{-1} \tag{11}$$

So, the minimum rain rate, considered for the estimation of the system gain bias, is 14mm/hr equivalent to 11dBR in dB scale for both radars. The perfect agreement of the two rain rate estimations is represented by the 1:1 line. In the density scatter plot, the total number of data, the bisector, the fit outputs (uncertainty, intercept and the correlation coefficient) and the computed bias are displayed. Thus, the self-consistency technique is performed on 28 July 2014, when thunderstorm cells interested the Piedmont and Ligurian regions. Figure 6 shows the density scatter plot of rain rates calculated on Bric della Croce data. For rain rates above 11dBR, there is an overall fair agreement, with the highest density of data below the 1:1 line. The computed system gain bias is slightly negative: -0.9dB.

Figure 7 displays the density scatter plot of rain rates calculated on Monte Settepani data. For rain rates above 11dBR, the

Atmos. Meas. Tech. Discuss., doi:10.5194/amt-2016-36, 2016
Manuscript under review for journal Atmos. Meas. Tech.
Published: 15 February 2016

Atmospheric Measurement Techniques Discussions

higher amount of data is located above the 1:1 line, pointing out the overestimation of the Z and Z_{dr}-based rain rate. The computed system gain bias is positive: 1dB.

The radar absolute calibration is also checked at the end of the study period on 13 October 2014. During this event a flood occurred in the south-eastern Piedmont (Arquata Scrivia), about 30 km north of Genova, with 24 hours cumulative precipitation exceeding 400mm (Fig. 8).

Figure 9 represents the rain rates density scatter plot in logaritmic scale for Bric della Croce radar, showing a remarkable density pattern around the bisector. The computed system gain bias is -0.5dB. For Monte Settepani radar, Fig. 10 shows the corresponding rain rates density plot. Due to the different geometric view of the storm, in this case the distribution of the observations in the polar domain is dominated by moderate rain rates, although for heavy rainfall the agreement is quite good, with a computed system gain of only -0.1dB. The results of the self-consistency procedure are summarized in Table 4.

4.2 Monitoring of the radar calibration stability

Between the two absolute calibration checks, the radar calibration is monitored by the ground clutter calibration and the Sun calibration. In addition, during precipitation, the intercalibration procedure is performed.

4.2.1 Intercalibration

Whenever precipitation is occuring on the overlaping area between the two radars, the intercalibration is performed as described in Sect. 3.2. The intercalibration results are displayed as:

- a density scatter plot of all the reflectivity data;
- a density scatter plot of the reflectivity pairs acquired below the melting layer and in dry-radome conditions. In this analysis, only reflectivity pairs associated to $\rho_{hv} > 0.95$ are considered in order to select only measurements in rain medium. Since different path inside the melting layer may experience different attenuation, the data are selected below the freezing level retrieved from numerical weather prediction (NWP) models to reduce the uncertainty introduced by the melting layer. In addition, the radome may attenuate the electromagnetic radiation during heavy rain, therefore the reflectivity data measured during rain above any of the two radars are removed, using a threshold of 20dBZ on the mean value of the reflectivity measured close to the radar.

For each density scatter plot, a linear fit is computed with 1:1 slope. If the radar calibration degrades, the system bias appears as a nonzero intercept value of the fit. The amount of scatter may vary depending of several factors, including the temporal and spatial alignment of the observations and the type of the precipitation (stratiform vs. convective). In the figures, the total number of data, the residual standard error of the fit ($Sigma$), the intercept value and the linear correlation coefficient R are displayed. In Fig. 11, the intercalibration performed on 28 July 2014 is displayed. First, the intercalibration is executed without thresholds on the copolar correlation coefficient, including all reflectivity irrespective of the heigth relative to the freezing level. In Fig. 11 left, the highest density of reflectivity pairs, denoted with warm colors, is located above the 1:1 line (black) and the total number or reflectivity pairs is about 56,000. A linear fit is applied on the reflectivity pairs with slope fixed at one and

Atmos. Meas. Tech. Discuss., doi:10.5194/amt-2016-36, 2016
Manuscript under review for journal Atmos. Meas. Tech.
Published: 15 February 2016

the computed intercept is about 4dBZ with a fit uncertainty of about 6dB. Then, the reflectivity pairs are filtered according the selection criteria aforementioned. In Fig. 11 right, the highest density of reflectivity is closer to the 1:1 line and the total number of data is about 4,000. Hence, the selection criteria have reduced the total number of reflectivity pairs by about an order of magnitude. The intercept is 2.4dBZ and the fit uncertainty has been reduced to about 4dB. Therefore, the intercept value is positive, meaning that the Monte Settepani radar overestimates the radar reflectivity values of rainfall when compared to the Bric della Croce radar.

4.2.2 Ground clutter calibration

The online hydrometeor classification processing allows to select the polar volumes without meteorological echoes for application of the ground clutter calibration. The output of the daily calibration is the set of the individual ground clutter ECDFs, from which suitable visualizations may be implemented for ease of online monitoring. In the current implementation, the image of the daily ECDFs of horizontal and vertical reflectivity with the enlargement around the 95^{th} quantile are displayed. In addition the historical trend of the daily average 95^{th} is produced as a time-series plot.

It has been observed that the clutter echoes ECDF may not have a steep slope around the 95^{th} quantile, depending on the nature of the clutter echoes. Especially for Monte Settepani radar, it has been noted that the slope of clutter echoes ECDF yields to a high uncertainty of the daily mean value of the 95^{th} quantile. Therefore, we empirically investigated a threshold on the clutter reflectivity in order to increase the ECDF slope around the 95^{th} quantile by removing weak clutter echoes. The threshold is imposed at 20dBZ, corresponding to the best compromise between the ECDF slope and the amount of clutter echoes.

Figure 12 is an example of ground clutter calibration in normal operational conditions: the 95^{th} quantile values of Z_H and Z_V are very similar and the spread of the individual ECDFs around the 95^{th} quantile is quite narrow. Comparing the enlargement around the 95^{th} quantile, the ECDFs of the horizontal polarization channel reaches the 95^{th} quantile at a value about 0.5dB lower than the vertical polarization channel. The historical trend from 28 July to 13 October 2014 shows a remarkable stability of the radar calibration (Fig. 13). The variability of the difference between to two channels is also quite limited over the study period and always within the standard deviation of the daily sample.

4.2.3 Sun calibration

Every five days, the radar calibration is operatively monitored by the Sun calibration, performed on the previous five days. The daily number of detected solar interferences depends on the season, i.e. on the ascent/descent rate of the Sun, on the solar activity, on scanning strategy, and on the sensitivity of the radar receiver. This procedure has been applied to both radars, but following the results of the Monte Settepani Sun calibration are reported.

During September 2014, the Monte Settepani radar collected 130 solar interferences, represented in the scatterplot of Fig. 14. The x-axis represents the $\Delta azimuth$ (see Sect. 3.4), the y-axis the $\Delta elevation$ and the colors the received power in dBm. The iso-lines show the value of the received power in a given point on the $\Delta azimuth - \Delta elevation$ plane, computed by the

Atmos. Meas. Tech. Discuss., doi:10.5194/amt-2016-36, 2016
Manuscript under review for journal Atmos. Meas. Tech.
Published: 15 February 2016

Atmospheric Measurement Techniques Discussions

theoretical model fit. It is evident that the solar interferences are scattered over roughly 1° in both azimuth and elevation around the antenna pointing, the black rhombus in figure. The calculated bias in azimuth and elevation, the Mean Squared Error and the Z_{dr} bias are reported in the figure.

The solar interferences are also analyzed to evaluate the receiver calibration, in addition to the antenna pointing accuracy during the study period. The computed power at the top of the atmosphere (P_{TOA}) is shown together with the reference values form DRAO in Fig. 15. The computed value of the power at the top of the atmosphere seen by the radar from the daily solar interferences is displayed with the fit uncertainty. The P_{TOA} values have been chosen as the quantity to be compared with the DRAO reference since it is calculated by the theoretical model and it represents the solar power received by the radar when the antenna beam is centered on the Sun. The reference values are considered without uncertainty. The numbers above the x-axis represent the number of interferences on which the mean and uncertainty are calculated. The days with missing values are due to a radar hardware failure. The daily P_{TOA} value of the received solar power is generally comparable with the DRAO reference. The azimuthal and elevation biases are computed by the three parameters model inversion (Altube et al., 2015). The azimuth bias and elevation bias from July 2014 to October 2014 are displayed in Fig. 16. The azimuth and elevation biases are both slightly negative, but approximately constant during the whole period. The Sun calibration also allows to monitor the values of the differential reflectivity. As previously mentioned, the solar Z_{dr} should be zero since the Sun is an unpolarized source of microwave radiation. The daily value of the solar Z_{dr} is shown in Fig. 17, where the error bars represent the standard deviation calculated on the data of the given day. The mean value of the daily Z_{dr} values is significantly deviating from the expected 0dB value. This bias is considered to correct the Z_{dr} measurements in the radar post-processing chain.

5 Discussion and conclusions

Four different procedures have been considered to operationally monitor the radar calibration, namely: self-consistency, ground clutter calibration, intercalibration and Sun calibration. The proposed approach for online monitoring consists in the integration of the results of the discussed calibration techniques. The study period has been chosen between 28 July 2014 and 13 October 2014 and the measurements have been acquired by the radars managed by Arpa Piemonte, Bric della Croce and Monte Settepani radars, considering the operational volume scans with 10 minutes update frequency.

Figure 18 provides a comprehensive view of the results achieved using the calibration monitoring techniques. This combined visualization represents an effective tool to operationally monitor and detect eventual drifts in the radar calibration, allowing a quick and efficient interpretation of the results obtained with the individual techniques. The reference absolute calibration is provided by the self-consistency technique. This technique is influenced by the adopted drop shape model and variability of the drop size distribution (DSD): in particular, different DSDs can produce up to 3-4dB difference in the reflectivity estimates (Ryzhkov et al., 2005). The proposed approach considers observations collected over a whole day, disregarding weak rainfall intensity data, where K_{dp} is excessively affected by noise. This allows to reduce the impact of DSD variations. In addition, the interpretation of the self-consistency results is favored by the integration with the calibration monitoring techniques.

Atmos. Meas. Tech. Discuss., doi:10.5194/amt-2016-36, 2016
Manuscript under review for journal Atmos. Meas. Tech.
Published: 15 February 2016

For Bric della Croce radar, a system bias less than 1dB, has been found using the self-consistency, with a change of about 0.5dB between 28 July 2014 and 13 October 2014. The ground clutter and Sun calibration of the Bric della Croce radar, Fig. 18 top, show a good stability of the radar calibration. The Sun calibration, however, displays the effect of interferences from artificial radio sources in the calibration monitoring. From 10 to 20 September, the uncertainty associated with the daily calibration increased abruptly. This anomalous variability was related to the appearance of new interferences from artificial radio sources, which eventually desappeared after several days. In this period, the computed solar power is higher than the DRAO reference and the uncertainty is considerably higher than in the other days.

For Monte Settepani radar, the self-consistency calibration allowed to estimate a system gain bias of 1dB (28 July 2014) and of -0.1dB (13 October 2014). The intercalibration and the Monte Settepani ground clutter calibration, Fig. 18 middle and bottom, suggest that the study period may be divided into three sections: from 28 July to 12 August; from 12 August to 17 September; from 17 September to 13 October. Until 12 August, the mean value of Monte Settepani ground clutter 95^{th} percentile is 57dB, and during rainfalls the Monte Settepani radar overestimates the radar reflectivity of about 2dB when compared to the Bric della Croce radar. On 12 August, a transmitter module broke down and the radar continued the normal operations with a lower pulse power due to a decrease of the Klystron cathode current. In fact, the ground clutter calibration shows a step between 11 and 12 August and the 95^{th} percentile of the reflectivity ECDF decreases at 54.7dB. In the same period the intercalibration shows the Monte Settepani underestimation of the radar reflectivity. The 4 September a second module broke down and the radar stopped. The radar was repaired 17 September, when two transmitter modules were substituted. Nevertheless, the ground clutter calibration from 17 September to 13 October displays a mean value of 56dB, 1dB lower than the mean value until 12 August. This difference is also pointed out by the self-consistency as a decrease of about 1dB in the system gain bias between 28 July to 13 October (Table 4). On the other hand, the receiving chain Sun calibration results show a fair agreement between the solar power at the top of the atmosphere as seen by the radar and the DRAO reference.

The decrease of the Monte Settepani system bias is 1.1dB. Even if this value is lower than the self-consistency accuracy, this change is also found in the ground clutter calibration from the difference between the mean value of the 95^{th} quantile of clutter echoes reflectivity averaged before 12 August and after 17 September. The integrated calibration approach then suggests that this change in the absolute calibration of the radar should not be ascribed to the self-consistency uncertainty, but may likely be related to some change in the transmitter subsystem during the corrective maintenance on 17 September.

Each calibration procedure is able to monitor a specific part of the radar system (e.g receiving chain, transmitting chain, antenna pointing, polarization channels) and the self-consistency technique allows to estimate the absolute calibration of the radar. The advantages of this integrated approach are 1) the extensive use of operational routines, that do not require to stop the radar, and 2) the integration of the results of several techniques exploiting different targets (ground clutter, Sun, rainfall) and based on different measurements (reflectivity only, polarimetric observations). The self-consistency procedure has been applied in this preliminary work on selected case studies with a large amount of heavy rainfall data. For an automated implementation of the procedure, more work is needed in particular to derive robust automatic data selection criteria. Overall, the integrated approach showed a capability to detect calibration losses, which may not be detected by a single calibration monitoring technique with the same level of confidence.

Atmos. Meas. Tech. Discuss., doi:10.5194/amt-2016-36, 2016
Manuscript under review for journal Atmos. Meas. Tech.
Published: 15 February 2016

Atmospheric Measurement Techniques Discussions

Acknowledgements. The work has been in part supported by a grant, D.D. n°1243 of 20 December 2013, by the Italian National Civil Protection. The participation of V. Chandrasekar is supported by the DOE-ASR program.

Atmos. Meas. Tech. Discuss., doi:10.5194/amt-2016-36, 2016
Manuscript under review for journal Atmos. Meas. Tech.
Published: 15 February 2016

Atmospheric Measurement Techniques Discussions

References

Altube, P., Bech, J., Argemi, P., Rigo, T., and Pineda, N.: Weather radar online Sun-monitoring in presence of leverage outliers: five or three parameter model inversion?, in: ERAD 2014 - The eighth European conference on radar in meteorology and hydrology, 2014.

Altube, P., Bech, J., Argemí, O., and Rigo, T.: Quality control of antenna alignment and receiver calibration using the Sun: adaptation to mid range weather radar observations at low elevation angles, Journal of Atmospheric and Oceanic Technology, 2015.

Beard, K. and Chuang, C.: A New Model for the Equilibrium Shape of Raindrops, Journal of the atmosperic sciences, p. 16, 1987.

Bechini, R. and Chandrasekar, V.: A Semisupervised Robust Hydrometeor Classification Method for Dual-Polarization Radar Applications, Journal of Atmospheric and Oceanic Technology, 32, 22–47, 2015.

Bringi, V. N. and Chandrasekar, V.: Polarimetric Doppler Weather Radar, principles and applications, Cambridge University Press, 2001.

Bringi, V. N., Chandrasekar, V., Balakrishnan, N., and Zrnic, D. S.: An Examination of Propagation Effects in Rainfall on Radar Measurements at Microwave Frequencies, J. Atmos. Oceanic Technol., 7, 829–840, 1990.

Gabella, M., Sartori, M., Boscacci, M., and Germann, U.: Vertical and Horizontal Polarization Observations of Slowly Varying Solar Emissions from Operational Swiss Weather Radars, Atmosphere, 6, 50–59, 2014.

Gorgucci, E., Scarchilli, G., and Chandrasekar, V.: Calibration of radars using polarimetric techniques, Geoscience and Remote Sensing, IEEE Transactions on, 30, 853–858, 1992.

Gorgucci, E., Scarchilli, G., Chandrasekar, V., and Bringi, V.: Rainfall estimation from polarimetric radar measurements: Composite algorithms immune to variability in raindrop shape-size relation, Journal of Atmospheric and Oceanic Technology, 18, 1773–1786, 2001.

Holleman, Huuskonen, I., A., Kurri, M., and Beekhuis, H.: Operational Monitoring of Weather Radar Receiving Chain Using the Sun, Journal of Atmosperic and Oceanic Technology, pp. 159–166, 2010.

Holleman, I. and Beekhuis, H.: Weather radar monitoring using the sun, Tech. rep., KNMI Koninklijk Nederlands Meteorologisch Instituut, De Bilt, technical report: TR-272, KNMIAUT2004 ISBN 9036922615 ISSN 01691708, 2004.

Rinehart, R. E.: Radar for Meteorologists, Rinehart Publications, 4 edn., 2004.

Ryzhkov, A. V., Giangrande, S. E., Melnikov, V. M., and Schuur, T. J.: Calibration issues of dual-polarization radar measurements, Journal of Atmospheric and Oceanic Technology, 22, 1138–1155, 2005.

Scarchilli, G., Gorgucci, E., Chandrasekar, V., and Dobaie, A.: Self-consistency of polarization diversity measurement of rainfall, Geoscience and Remote Sensing, IEEE Transactions on, 34, 22–26, 1996.

Silberstein, D., Wolff, D., Marks, D., Atlas, D., and Pippit, J.: Ground Clutter as a Monitor of Radar Stability at Kwajalein, RMI, Journal of Atmosperic and Oceanic Technology, p. 2037, 2008.

Tapping, K.: Antenna calibration using the 10.7 cm solar flux, in: Workshop on Radar Calibration, Albuquerque, NM, 2001a.

Tapping, K.: Antenna Calibration Using the 10.7cm Solar Flux, in: Workshop on Radar Calibration, Abuquerque, AMS, 2001b.

Testud, J., Bouar, E. L., Obligis, E., and Ali-Mehenni, M.: The rain profiling algorithm applied to polarimetric weather radar, J. Atmos. Oceanic Technol., 17, 332–356, 2000.

Ulbrich, C. W.: Natural variations in the analytical form of the raindrop size distribution, Journal of Climate and Applied Meteorology, 22, 1764–1775, 1983.

Wang, Y. and Chandrasekar, V.: Algorithm for estimation of the specific differential phase, Journal of Atmospheric and Oceanic Technology, 26, 2565–2578, 2009.

Atmos. Meas. Tech. Discuss., doi:10.5194/amt-2016-36, 2016
Manuscript under review for journal Atmos. Meas. Tech.
Published: 15 February 2016

Atmospheric Measurement Techniques Discussions

Whiton, R. C., Smith, P. L., and Harbuck, A. C.: Calibration of weather radar systems using the sun as a radio source, in: 17th Conference on Radar Meteorology, pp. 60–65, 1976.

Wolff, D. B., Marks, D. A., and Petersen, W. A.: General Application of the Relative Calibration Adjustment (RCA) Technique for Monitoring and Correcting Radar Reflectivity Calibration, Journal of Atmospheric and Oceanic Technology, 2015.

Atmos. Meas. Tech. Discuss., doi:10.5194/amt-2016-36, 2016
Manuscript under review for journal Atmos. Meas. Tech.
Published: 15 February 2016

Atmospheric Measurement Techniques Discussions

Table 1. Radars locations.

	Bric della Croce	**Monte Settepani**
Municipality	Pecetto Torinese (TO)	Calizzano (SV)
Altitude (m)	736	1,386
Latitude	45.03	44.25
Longitude	7.73	8.20

Atmos. Meas. Tech. Discuss., doi:10.5194/amt-2016-36, 2016
Manuscript under review for journal Atmos. Meas. Tech.
Published: 15 February 2016

Atmospheric Measurement Techniques Discussions
Open Access
EGU

Table 2. Technical specifications of the radars dealt in this work.

	Bric della Croce	**Monte Settepani**
Polarization	Linear H/V Simultaneous mode	Linear H/V Alternate mode
Measured parameters	Z, Z_{dr}, Φ_{dp}, K_{dp}, ρ_{hv} and V	Z, Z_{dr}, Φ_{dp}, K_{dp}, ρ_{hv} and V
Antenna diameter (m)	4.2	4.2
Beam width (°)	0.94	0.94
Maximum sidelobe level (dB)	-28	-28
Antenna gain (dB)	44.5	44.5
Transmitter	Magnetron	Klystron
Transmitted frequency (MHz)	5,640	5,620
Peak power (KW)	$\simeq$250	$\simeq$250
Pulse length (μs)	0.5, 2.0	0.5, 1.5, 3.0
PRF (HZ)	250÷1,200	300÷2,000

Atmos. Meas. Tech. Discuss., doi:10.5194/amt-2016-36, 2016
Manuscript under review for journal Atmos. Meas. Tech.
Published: 15 February 2016

Atmospheric Measurement Techniques Discussions

Table 3. Summary of parameters used in the Sun calibration. The radar beam width is referred to the C-band radars managed by Arpa Piemonte.

Parameter	Value
Gaseous attenuation, a (dB km^{-1})	0.019
$4/3$ Earth's radius, R_E (km)	8,495
Solar beam width, Δ_s ($^\circ$)	0.54
Radar beam width, Δ_r ($^\circ$)	0.94
Azimuthal bin size, Δx ($^\circ$)	1

Atmos. Meas. Tech. Discuss., doi:10.5194/amt-2016-36, 2016
Manuscript under review for journal Atmos. Meas. Tech.
Published: 15 February 2016

Atmospheric Measurement Techniques Discussions

Table 4. System gain biases computed by the self-consistency procedure for Bric della Croce and Monte Settepani radars.

Date	Bric della Croce	Monte Settepani
28 July 2014	-0.91dB	0.95dB
13 October 2014	-0.49dB	-0.13dB

Atmos. Meas. Tech. Discuss., doi:10.5194/amt-2016-36, 2016
Manuscript under review for journal Atmos. Meas. Tech.
Published: 15 February 2016

Atmospheric Measurement Techniques Discussions

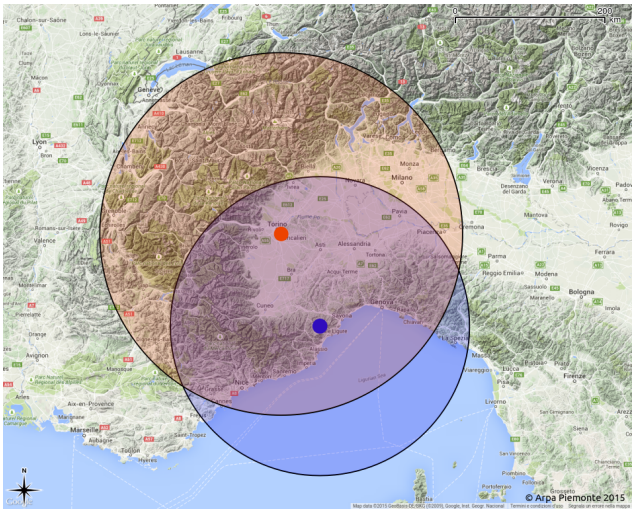

Figure 1. Weather radars in North-Westerner Italy. The circles correspond to the scan domains and the colors are related to the markers in the map. The red and blue markers represent the two C-band radar locations. The circles represent the Bric della Croce scan (red) and the Monte Settepani scan (blue).

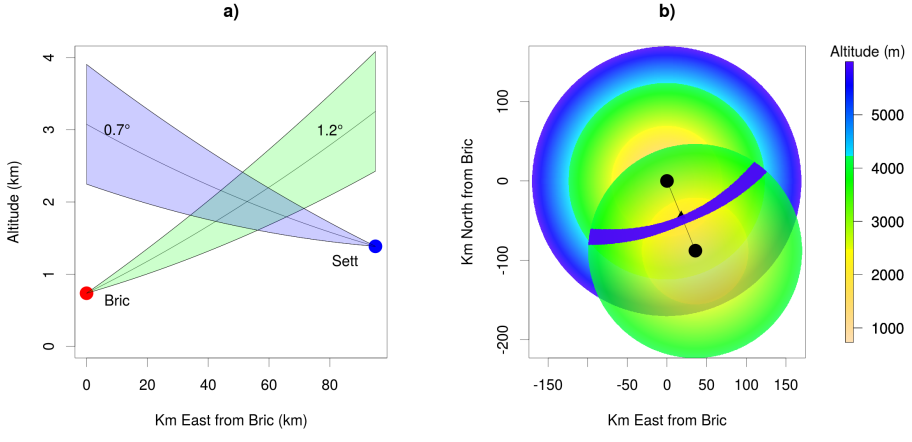

Figure 2. Intersection (a) of Bric della Croce (red point) and Monte Settepani (blue point) radar beams for elevations 0.7° (Bric della Croce) and 1.2° (Monte Settepani). The overlapping volume is about halfway between the two radars. Ground projection of the overlapping volume (b) of Bric della Croce radar (elevation angle 1.2°) and Monte Settepani radar (elevation angle 0.7°). Bric della Croce radar is the northernmost. The colors represent the altitude in meters of the main beam center axis. The triangle is located halfway between Bric della Croce and Monte Settepani radars.

Atmos. Meas. Tech. Discuss., doi:10.5194/amt-2016-36, 2016
Manuscript under review for journal Atmos. Meas. Tech.
Published: 15 February 2016

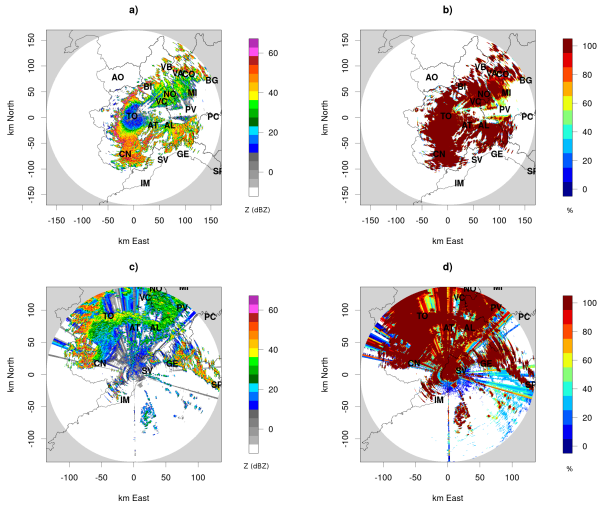

Figure 3. Mean reflectivity value and frequency of clutter echoes collected by Bric della Croce (figures a and b) and by Monte Settepani (figures c and d) radars at the lowest elevations, -0.1° and -0.3° respectively. The maximum value exceeds 64dBZ and 100% represents very stable echoes.

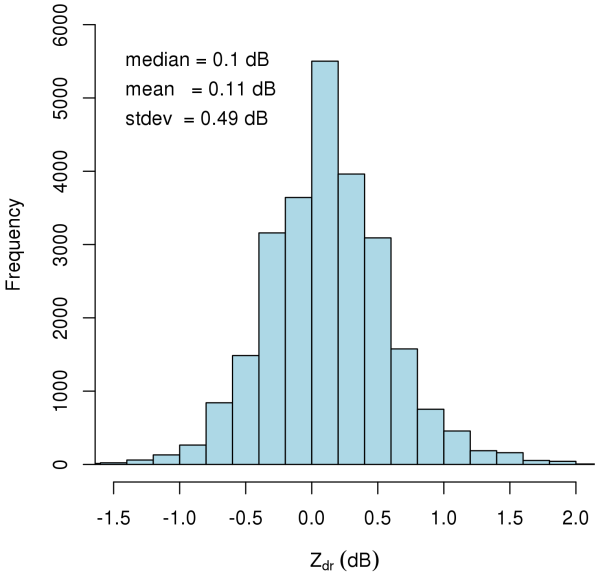

Figure 4. Histogram of differential reflectivity echoes satisfying the selection criteria. Bric della Croce radar, 13^{th} October 2014.

Atmos. Meas. Tech. Discuss., doi:10.5194/amt-2016-36, 2016
Manuscript under review for journal Atmos. Meas. Tech.
Published: 15 February 2016

Atmospheric Measurement Techniques Discussions

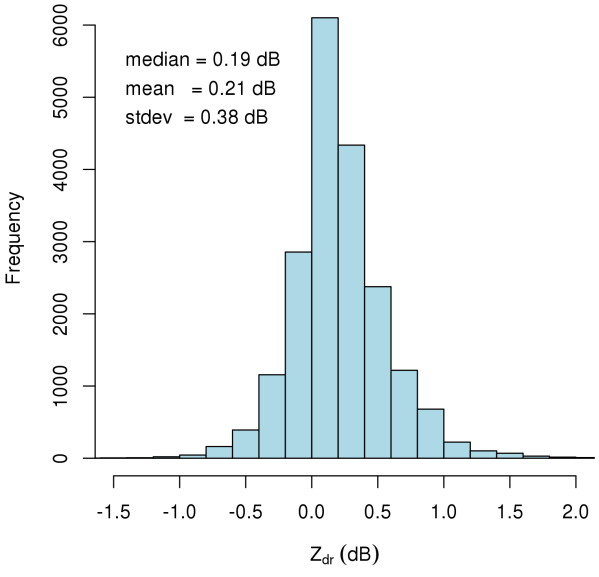

Figure 5. As in Fig. 4, but for Monte Settepani radar, 10^{th} October 2014.

Atmos. Meas. Tech. Discuss., doi:10.5194/amt-2016-36, 2016
Manuscript under review for journal Atmos. Meas. Tech.
Published: 15 February 2016

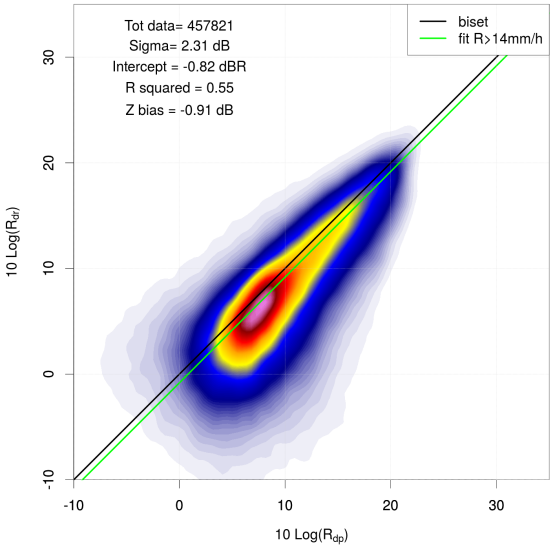

Figure 6. Self consistency procedure applied on Bric della Croce radar, 28^{th} July 2014. The K_{dp}-based rain, in dB scale, is shown in the x-axis and the rain rate based on Z and Z_{dr}, in dB scale, in the y-axis. The colors represent the density of data from blue (low density) to violet (high density). The black and green line display the 1:1 line and the fit with slope set at one, performed on the data with rain rate greater than 14mm/hr. The total number of data, the fit uncertainty, the intercept value (in dB), the correlation coefficient and the computed system bias are reported in the plot.

Atmos. Meas. Tech. Discuss., doi:10.5194/amt-2016-36, 2016
Manuscript under review for journal Atmos. Meas. Tech.
Published: 15 February 2016

Atmospheric Measurement Techniques Discussions

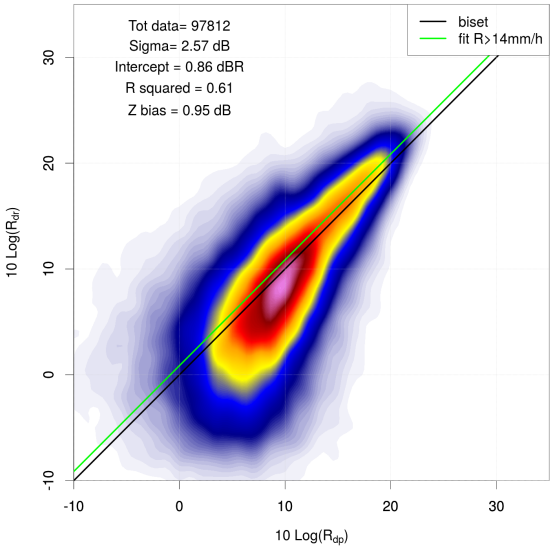

Figure 7. As in Fig. 6, but for Monte Settepani radar.

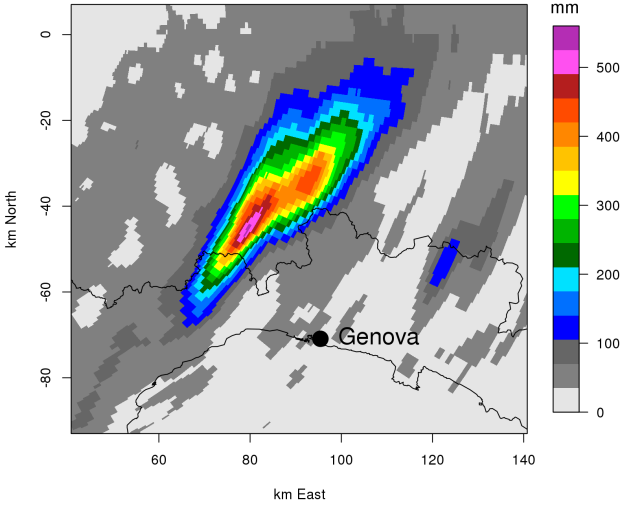

Figure 8. 24-hours cumulative precipitation in mm (color scale) from Bric della Croce radar on 13^{th} October 2014. The axes display the East and North distances from the radar. The black point refers to the city of Genova.

Atmos. Meas. Tech. Discuss., doi:10.5194/amt-2016-36, 2016
Manuscript under review for journal Atmos. Meas. Tech.
Published: 15 February 2016

Atmospheric Measurement Techniques Discussions

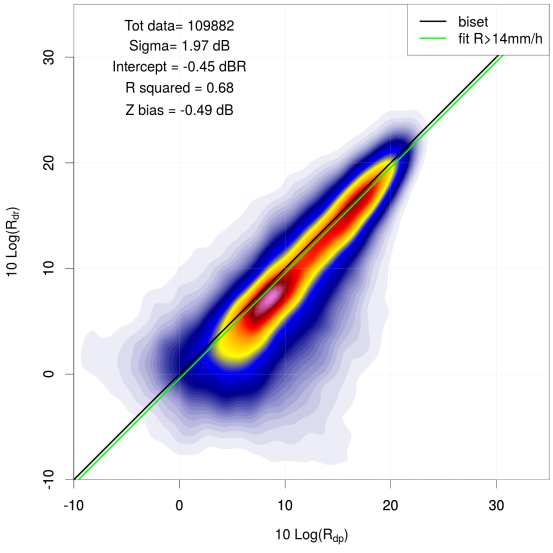

Figure 9. As in Fig. 6 but for the Bric della Croce radar, 13^{th} October 2014.

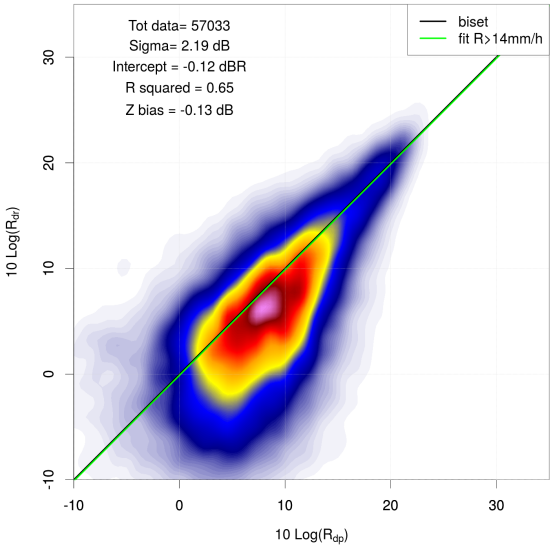

Figure 10. As in Fig. 6 but for the Monte Settepani radar, 13^{th} October 2014.

Atmos. Meas. Tech. Discuss., doi:10.5194/amt-2016-36, 2016
Manuscript under review for journal Atmos. Meas. Tech.
Published: 15 February 2016

Atmospheric Measurement Techniques Discussions

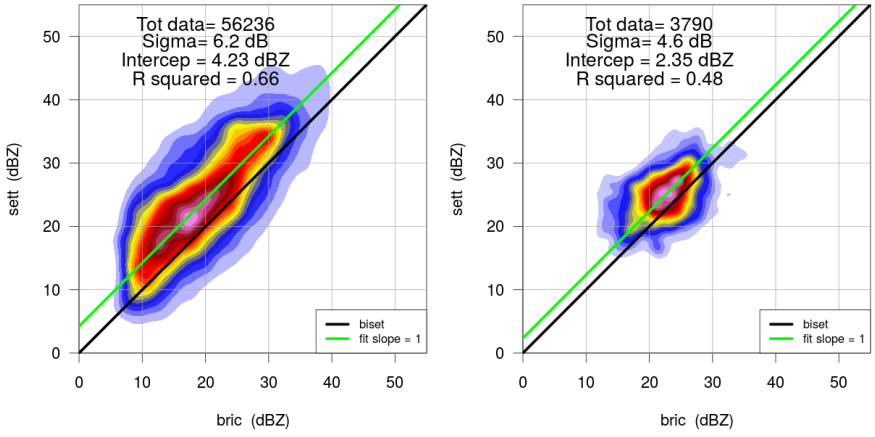

Figure 11. Intercalibration between Bric della Croce and Monte Settepani, 28 July 2014. Comparison considering all the reflectivity pairs (left) and the reflectivity pairs, associated to $\rho_{hv} > 0.95$, acquired during dry-radome conditions and below the melting layer (right).

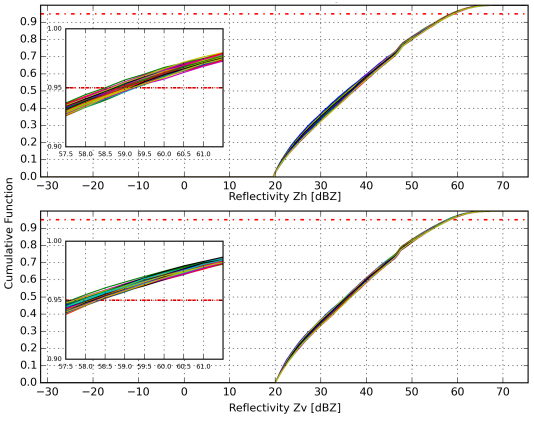

Figure 12. Z_h and Z_v ECDF with respective enlargements around the 95^{th} quantile, Bric della Croce radar at elevation 0.5°, 7 October 2014.

Atmos. Meas. Tech. Discuss., doi:10.5194/amt-2016-36, 2016
Manuscript under review for journal Atmos. Meas. Tech.
Published: 15 February 2016

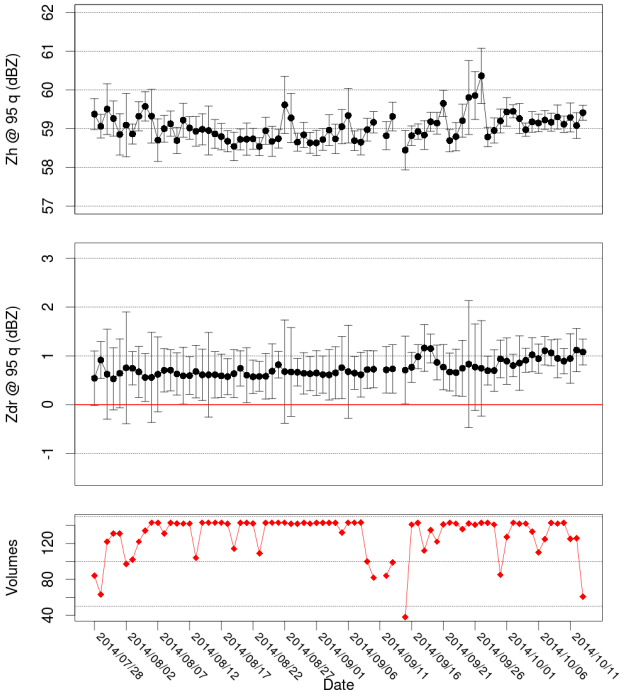

Figure 13. Mean values of the daily values of the 95^{th} quantile of Z_H (top) and Z_{dr} (center) ECDFs. The bottom plot shows the number of scans used to compute the daily mean values. The error bars represents the standard deviation.

Atmos. Meas. Tech. Discuss., doi:10.5194/amt-2016-36, 2016
Manuscript under review for journal Atmos. Meas. Tech.
Published: 15 February 2016

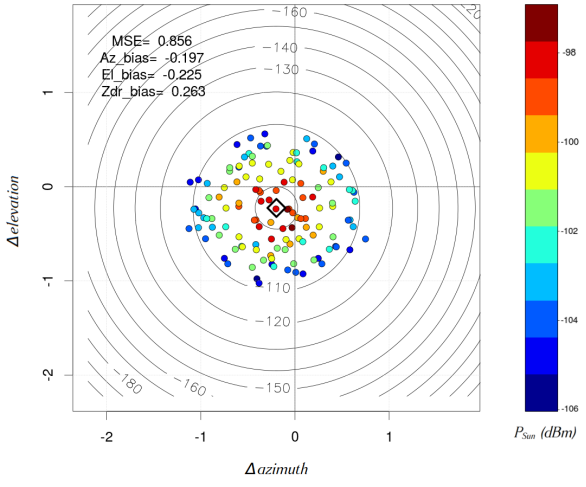

Figure 14. Scatter plot of solar interferences collected by the Monte Settepani radar during September 2014. The x-axis represent the $\Delta azimuth$, the y-axis the $\Delta elevation$ and the colors the received power in dBm. The iso-lines show the value of the received power in a given point on the $\Delta azimuth - \Delta elevation$ plane, computed by the theoretical model fit. The black rhombus is the antenna pointing. The calculated bias in azimuth and elevation, the Mean Squared Error and the Z_{dr} bias are reported in the figure.

Atmos. Meas. Tech. Discuss., doi:10.5194/amt-2016-36, 2016
Manuscript under review for journal Atmos. Meas. Tech.
Published: 15 February 2016

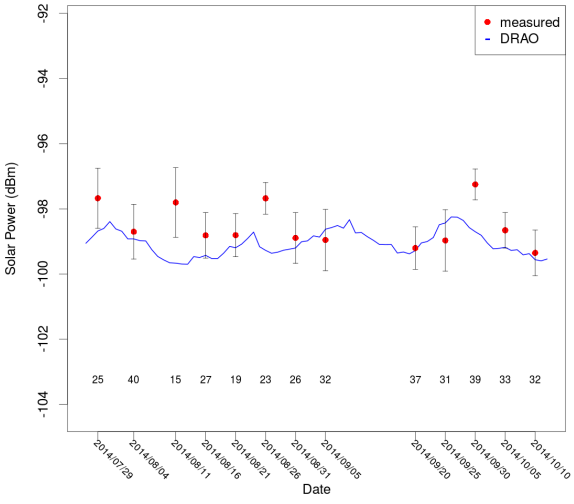

Figure 15. Daily analysis of the solar interferences detected by the Monte Settepani radar during July - October 2014. The value of the power at the top of the atmosphere (P_{TOA}) seen by the radar, computed from the daily solar interferences, is displayed as red points. The error bars are calculated as the square root of the differences between the measured solar power and the theoretical model. The blue points display the DRAO reference values of the solar power. The amount of the collected solar interferences for each day is shown by the numbers in the plot.

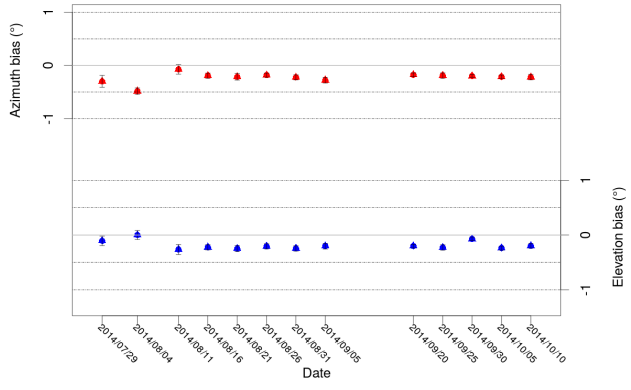

Figure 16. Daily analysis of azimuth bias (top) and elevation bias (bottom) of the Monte Settepani radar during July - October 2014.

Atmos. Meas. Tech. Discuss., doi:10.5194/amt-2016-36, 2016
Manuscript under review for journal Atmos. Meas. Tech.
Published: 15 February 2016

Atmospheric Measurement Techniques Discussions

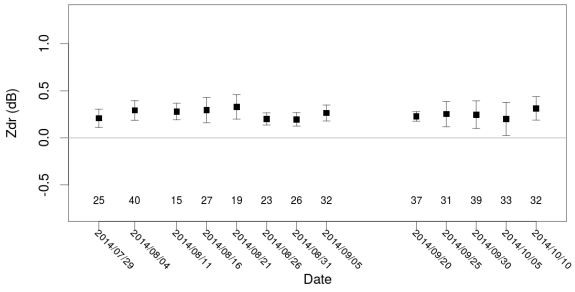

Figure 17. Daily analysis of the differential reflectivity of the solar interferences detected by the Monte Settepani radar during July - October 2014. The error bars represent the standard deviation of the daily Z_{dr} values.

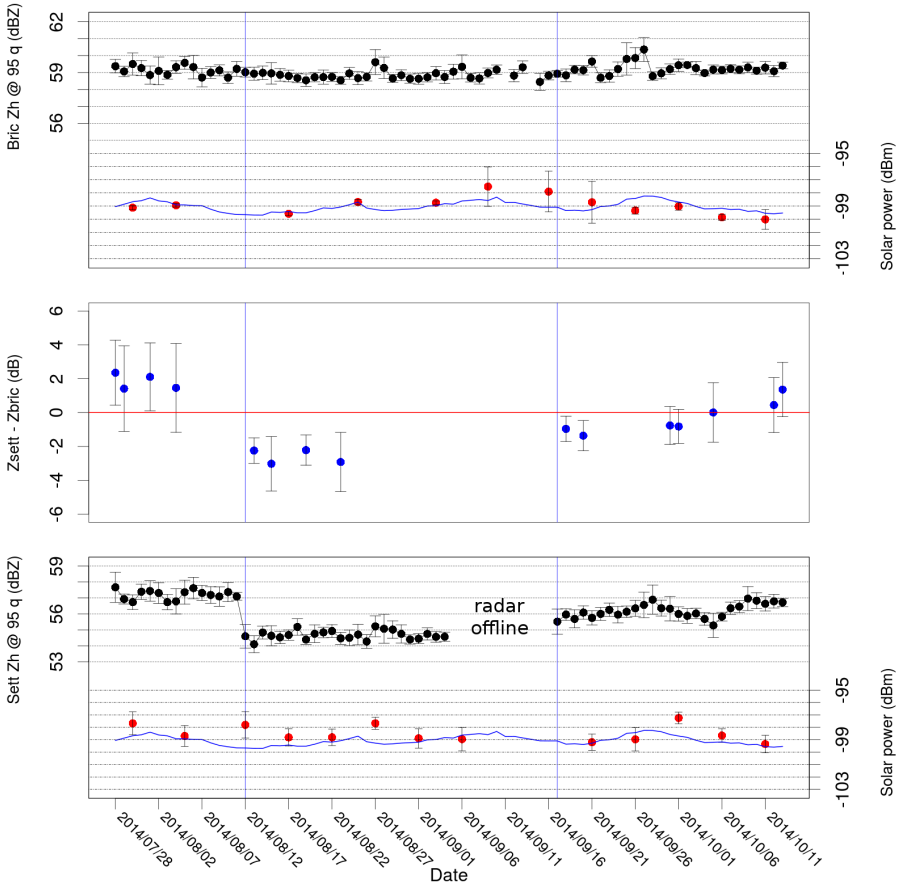

Figure 18. Monitoring the stability of radar calibration. From the top, Bric della Croce ground clutter and Sun calibrations; Bric della Croce and Monte Settepani intercalibration; Monte Settepani ground clutter and Sun calibrations. The error bars represent the estimated uncertainty. In the Sun calibration, the blue line shows the DRAO reference at 20:00UTC, as reported in Wolff et al. (2015).